Thin, Flexible Sensors and Actuators as 'Instrumented' Surgical Sutures for Targeted Wound Monitoring and Therapy

Dae-Hyeong Kim, Shuodao Wang, Hohyun Keum, Roozbeh Ghaffari, Yun-Soung Kim, Hu Tao, Bruce Panilaitis, Ming Li, Zhan Kang, Fiorenzo Omenetto, Yonggang Huang, and John A. Rogers*

Sutures are among the simplest and most widely used devices in clinical medicine. All existing synthetic and natural forms use thread-like geometries, as purely passive, mechanical structures that are flexible and resilient to tensile stress. Several recent reports describe strategies to incorporate advanced functionality into this platform through the employment of shape-memory polymers that offer mechanical actuation or through the release of bioresorbable compounds that carry growth factors and antibiotics to accelerate healing.[1–3] Such technologies lack, however, programmable actuation or sensory feedback control. Sutures that embed flexible sensors

Prof. D.-H. Kim
School of Chemical and Biological Engineering
WCU Program of Chemical Convergence for
Energy and Environment
Institute of Chemical Processes
Inter-University Semiconductor Research Center
Seoul National University
Seoul 151-741, Republic of Korea

Dr. S. Wang, H. Keum, Y.-S. Kim, Prof. J. A. Rogers
Department of Materials Science and Engineering
Beckman Institute for Advanced Science and Technology
and Frederick Seitz Materials Research Laboratory
University of Illinois at Urbana-Champaign
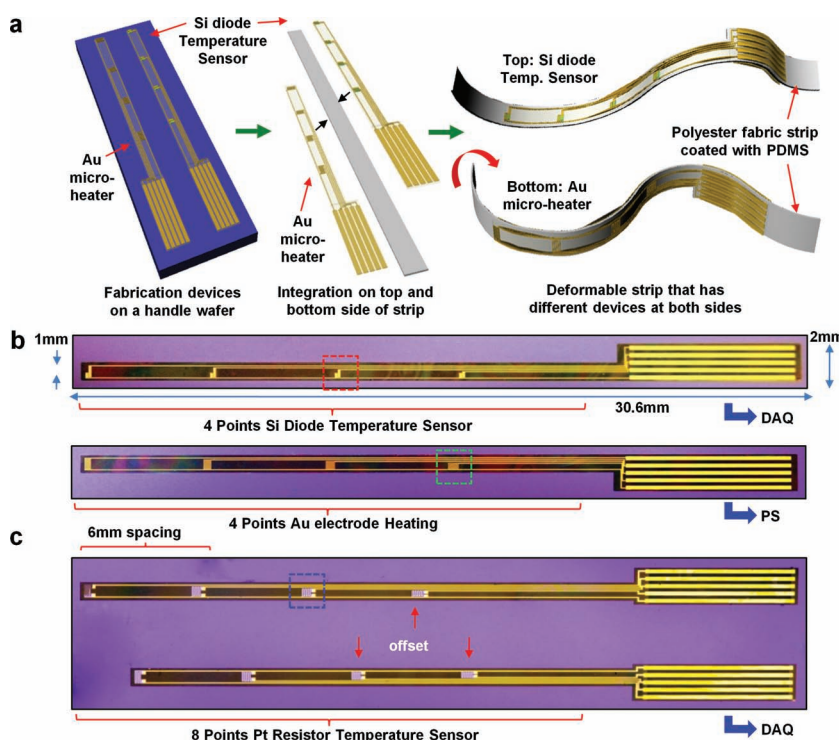Urbana, IL 61801, USA
E-mail: jrogers@illinois.edu

Dr. R. Ghaffari
MC10 Inc., 36 Cameron Avenue
Cambridge, MA 02140, USA

Dr. H. Tao, Dr. B. Panilaitis, Prof. F. Omenetto
Department of Biomedical Engineering
Tufts University, Medford, MA 02155, USA

M. Li, Prof. Z. Kang
State Key Laboratory of Structural Analysis for Industrial Equipment
Dalian University of Technology
Dalian 116024, China

Prof. Y. Huang
Department of Mechanical Engineering and Department
of Civil and Environmental Engineering
Northwestern University
Evanston, IL 60208, USA

and associated electronic circuits could perform these and other related functions. Demonstrations using thin flexible strips equipped with sensors for pressure and chemical monitoring have been reported[4,5] but not in designs for use as sutures. Furthermore, the organic and silver-based material components comprising these devices might limit their performance capabilities, and also lead to concerns about long-term durability in moist, dynamic conditions in the body. Here, we report strips with significantly smaller form factors, specifically engineered for use as flexible sutures (~1 mm width and ~3 μm thickness) 'instrumented' with high quality single crystal inorganic semiconductors of biocompatible materials such as silicon in nanomembrane formats.[6] The resulting class of technology offers routes to high levels of performance and sophisticated function in sensors and actuators suitable for *in vivo* use. This new type of diagnostic/therapeutic tools could monitor, sense and actuate in a manner coordinated with natural biological responses in the body for improved health outcomes.

The systems described in the following use ultrathin, narrow strips of biocompatible polymers as platforms for integrated single crystal silicon nanomembranes (Si NM) electronics and sensors, configured together in ways that provide requisite mechanical properties. The examples focus on measurement and delivery of heat, using systems composed of Si NMs, multicomponent metallization and dielectric interlayers/encapsulants, all in bifacial designs (i.e. devices and interconnects on both sides of a thin substrate). The collective properties, including operational compatibility with complete immersion in water and biofluids[7] and robustness to large stresses/strains that occur during suturing, are demonstrated through *in vivo* evaluations using animal models. The envisioned clinical context is for sensing and programmable delivery of local heating and electrical stimulation to promote healing of chronic wounds[8,9] or for heat shock strategies in cancer treatment.[10] Additional possibilities exist in thermally activated drug release from temperature sensitive, polymer host matrices as coatings onto these devices.[11]

A representative system includes Si NM diode temperature sensors and microscale Joule heating elements

Figure 1. Ultrathin suture strip with integrated temperature sensors and thermal actuators. a) Schematic illustration of steps for building the device and integrating them in a bifacial configuration on a thin, narrow strip of polyester coated with PDMS. b) Optical images of a 1 × 4 array of temperature sensors based on Si nanomembranes (top) and a 1 × 4 array of microheaters based on Au wires in a serpentine layout (bottom), both on a handle wafer. The small total thickness (<3 μm) and the neutral mechanical plane (NMP) design minimize strains induced by deformations. Five metal pads at the end connect either to a data acquisition system (DAQ) or a power supply (PS) through an anisotropic conductive film (ACF). c) Optical image of a temperature sensor array based on Pt resistors, on a handle wafer. The two arrays have four sensors each, which are arranged in a bifacial configuration, with an offset to provide an effective 1 × 8 array.

(**Figure 1**). The fabrication begins with microfabrication of interconnected components on a temporary, 'handle' substrate (silicon wafer coated with a thin layer of polymethylmethacrylate, PMMA), using a combination of conventional (e.g. photolithography, physical vapor deposition, reactive ion etching) and unconventional (e.g. transfer printing, nanomaterials assembly) techniques. The diodes contain p-n junctions created by selectively doped Si NMs, prior to release and transfer from a silicon-on-insulator wafer (SOI, 300 nm top silicon, p-type, SOITEC, France) to a thin layer of polyimide (PI, ~1.2 μm, Sigma Aldrich, USA) spin-cast on the handle substrate. Photolithographically defined traces of exposed metal serve as interconnects and contact pads. A thin spin-cast layer of epoxy (~1.5 μm, Microchem, USA) encapsulates the entire system. As a final step of fabrication, we dissolve the PMMA, which allows release of the strips from the mother wafer. Two additional transfer printing steps deliver a pair of separate strips formed in this way onto opposite sides of a thin, narrow polymer (polyester, synthetic fabric) substrate (coated with polydimethylsiloxane (PDMS, ~50 μm)), in an aligned configuration. Figure 1a provides a schematic illustration of fabrication processes in its entirety.

The narrow widths (~1 mm), ultrathin profiles (~3 μm) and meandering lengths (~30 mm) of these devices allow for exceptional mechanical flexibility. Multiple corkscrew-like twists and knots[12] are necessary for effective suturing. These geometrical features can be further optimized for the intended anatomy and targeted wound. At the proximal end of the strip, contact pads extend out to establish connections with metal traces that lead to anisotropic conductive films (ACF). Terminal connections to the ACF connections provide interfaces to external power supplies (PSs) and data acquisition consoles (DAQs). The example in Figure 1b integrates diagnostic functionality (i.e. temperature sensors; Si NM diodes) on one side of a strip and therapeutic functionality (i.e. resistive Joule heaters; Au serpentine traces) on the other. Alternatively, Figure 1c demonstrates a purely diagnostic system that combines temperature sensors (Pt NM, serpentine thermistors) on both sides in a staggered layout that improves the spatial coverage of the measurement to ~3 mm.

Figure 2a presents an optical micrograph (left) and current-voltage measurements (right) of a Si NM diode as a function of temperature, externally controlled by a hot plate. The results show the ability to measure small changes in body temperature (typically 3-4 °C) caused by inflammation[13] with temperature sensor resolution of ~0.2 °C. A representative Au micro-heater along with infrared thermal images collected during operation at two levels of heating is shown in Figure 2b. The thin substrate has exceptionally low thermal mass, thereby enabling efficient, localized delivery of heat to surrounding tissue. Replacing the Au micro-heater with Pt in a modified serpentine layout yields simple thermistors, as alternatives to the Si NM sensors (Figure 2c). As with the diodes, the resistance of the Pt devices changes linearly with temperature (right frame of Figure 2c). Furthermore, the effects of parasitic resistances because of the use of long wires can be ignored because changes in resistance of Pt thermistors are significantly larger than the resistances measured along the metal interconnects and bus lines leading to the DAQ. For the purpose of temperature measurement, Pt sensors offer advantages in simplicity of fabrication and reduced cost relative to more active Si-based approaches. Si NM diodes demonstrate the ability to integrate silicon into these platforms for more sophisticated levels of electronic function beyond those explicitly demonstrated here.[7]

The mechanics of these devices are central to their use in sutures. Designs must offer the required physical durability and deformability, while avoiding strains that could induce fracture in the functional materials. Reducing the likelihood
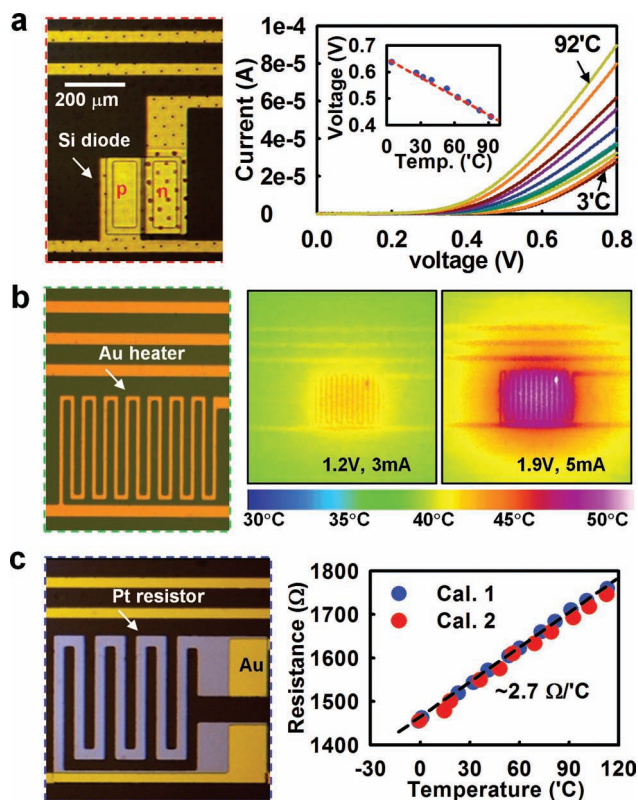
Figure 2. Images and characterization data from individual devices, with designs optimized for integration onto thin, narrow suture strips. a) Microscope image of a Si NM diode-based temperature sensor (left) and its characterization results (right). Voltage readings at constant current from current-voltage curves at different temperatures (right frame) show a linear behavior (inset). b, Microscope image of an Au microheater (left) and infrared camera images of heating produced at different currents (right). c, Microscope image of a Pt resistor-based temperature sensor (left) and its calibration results at different temperatures (right). The slope of the resistance versus temperature is ~2.7 Ω/ °C.

of fracture can be challenging, particularly when the devices incorporate brittle materials such as silicon (fracture strain ~ 1%). To avoid mechanical failure, thin, narrow geometries are beneficial because they can accommodate strains induced by bending. For example, plastic substrates used in typical flexible electronic devices (thicknesses ~100 μm) with standard, surface-mounted designs have bending stiffness characteristics that are two orders of magnitude greater than those associated with the sutures reported here. In addition, the top layer of epoxy positions the active materials within or near the neutral mechanical plane (NMP), thus further reducing strains in the most brittle elements (e.g. silicon).

The essential mechanical properties can all be captured quantitatively by simple calculations and modeling. A cross-section of a representative device appears in **Figure 3**a (left frame). The Young's moduli, thicknesses and widths of the different layers are denoted as E_i, h_i and w, respectively. The device elements (the golden or dark grey bricks shown in Figure 3a) are much thinner (50 ~ 150 nm) and narrower (40 μm) than the PI (h_{PI}= 1.2 μm, w = 1.0 mm) bottom and epoxy (h_{epoxy}=1.5 μm, w=1.0 mm) top layers; their influence on the bending characteristics are negligible (<0.2% error). The

bending stiffness of the suture in the width direction is given by

$$(EI) = \sum_{i=1}^{N} E_i h_i w \left[\left(y_0 - \sum_{j=1}^{i} h_j \right)^2 + \left(y_0 - \sum_{j=1}^{i} h_j \right) h_i + \frac{1}{3} h_i^2 \right], \quad (1)$$

where $N = 3$ is the number of layers and y_0 is the position of NMP (Figure 3a)

$$y_0 = \sum_{i=1}^{N} E_i h_i \left(\sum_{j=1}^{i} h_j - \frac{1}{2} h_i \right) \Bigg/ \sum_{i=1}^{N} E_i h_i, \quad (2)$$

and $E_1 = E_{PI} = 2.5$ GPa[14,15] $E_2 = E_{SiO2} = 73$ GPa,[16] $E_3 = E_{epoxy} = 4.4$ GPa,[17] $h_1 = h_{PI}$, $h_2 = h_{SiO2} = 50$ nm, $h_3 = h_{epoxy}$. The bending stiffness calculated from Equations (1-2) is 5.9×10^{-12} N·m², which is consistent with values (6.2×10^{-12} N·m²) obtained with finite element analysis (FEA). For many applications, the suture mainly undergoes various forms of bending (Figure 3b, c). The bending strain in the suture is expressed as

$$\varepsilon = \frac{|y|}{R}, \quad (3)$$

where y is the distance from the NMP (Figure 3a) and R is the bending radius. NMP is given by Equation (2) as $y_0 = 1.47$ μm, which is just 0.02 μm above the Au layer. As a result, the strain remains small even when the suture is in a bending state (e.g. $|\varepsilon| = 0.5\%$ in Pt when $R = 0.44$ mm).

A representative example of a smart suture strip containing temperature sensors and Au electrodes is shown in Figure 3b. The ultrathin design, the NMP configuration and the use of PDMS as a strain isolation layer on a polyester strip (Figure 3a, right frame) enable large deformations, such as those involved during suturing (second and third frame of Figure 3b) as well as knotting (last frame of Figure 3b). Since the PDMS layers are much softer and thicker (~250 kPa, 50 μm) than the device strips (>2 GPa, 2.7 μm), the PDMS (Figure 3a, right frame) absorbs most of the strain deformations that result from bending. The PDMS layer provides this strain isolation without significantly shifting the location of the NMP. For suturing (Figure 3b, middle frames), the bending radius at the most severely deformed region is estimated to be R~2 mm, giving rise to a maximum bending strain in the gold layer of 0.0085% (Equation 3), consistent with 0.0081% given by FEA (Figure 3d).

These fabrication sequences and device designs can accommodate a wide range of substrate materials. To achieve minimal thickness in a final, deployed state, bioresorbable materials, such as silk, can be used (middle frame of Figure 3c). The location of the NMP for a suture strip with Pt temperature sensors is schematically shown in the left frame of Figure 3c. Because of enhanced flexibility after dissolving the underlying silk substrate, folding around a thin glass slide (middle frame of Figure 3c) and wrapping around a fingertip (right frame of Figure 3c) are both possible. In the case of folding the suture around a sharp glass edge (thickness 1.3 mm) the bending radius of the suture at the sharp edge is estimated to be R~1.3 mm and the corresponding maximum strain given by Eq. (3) is 0.012% for the gold, consistent with 0.013% given by FEA (Figure 3e). The zigzag shape of
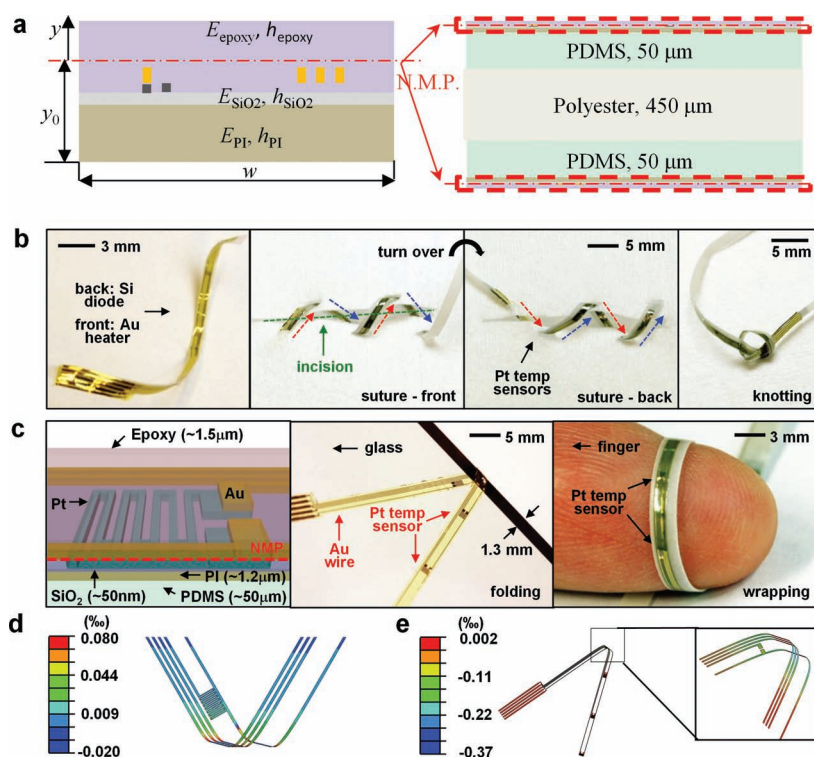
Figure 3. Mechanics of thin, instrumented suture strips. a) Schematic illustrations of the cross section of a bifacial suture. b) Optical image of a suture strip in its curled form (first frame) and after suturing (second and third frame) and knotting (last frame). c) Optimized mechanical structure shown in a schematic illustration (left frame) and examples of a device under various deformations, such as folding (center frame) and wrapping (right frame). d) Strain distribution for the deformation of Figure 3b (middle frame). e) Strain distribution for the deformation of Figure 3c (middle frame).

frame of Figure 4c shows a tapered strip knotted to a suture needle, following three stitch patterns. The four temperature sensors embedded in the strip measure local temperatures 25.1, 26.8, 26.1 and 25.9 °C from left to right.

Failure was avoided by limiting the fracture strains within the brittle materials (gold ~1%,[18] Pt ~4%,[19] epoxy ~6%,[20] PI ~6%).[21] Appropriate function is achieved only when the tensile strain is smaller than the smallest fracture strains listed above, i.e. $\varepsilon_f \approx 1\%$. Therefore the maximum tension the suture could provide is

$$T_{max} = \varepsilon_f \left(E A \right) = \varepsilon_f \cdot \sum_i E_i A_i \qquad (4)$$

where E_i and A_i are the Young's moduli and cross-section areas of different material layers (Epoxy–4.4 GPa,[17] 3.0×10^3 μm^2, SiO$_2$–73 GPa,[16] 100 μm^2, PI–2.5 GPa,[14,15] 2.4×10^3 μm^2, PDMS–250 kPa, 0.20 mm^2, polyester–580 MPa,[22] 1.0 mm^2), respectively. Using the experimental data, Equation (4) gives $T_{max} = 6.1$ N which is more than two times the tension needed (~2.5 N)[23] for suturing a 60 mm long incision. Therefore, the smart sutures shown in Figure 3a had sufficient tensile strength to be pulled through animal tissue with a suture needle. Other possible choices of substrate material could improve further the strength.

The materials and mechanics strategies developed in this study enable a new class of sutures with electronic 'instrumentation' for advanced functionality in monitoring the state of wound sites and, potentially, providing therapeutic operation. Sensing and therapy functions in sutures can exploit device-quality Si based elements, giving rise to a wide range of clinical applications, including delivery of light, chemical and electrical stimuli locally to wound sites.

the Pt sensor (Figure 2c) further reduces the strain in this material to only 0.0098% (obtained by FEA). In addition to minimizing the thickness of the residual, active devices, bioresorbable substrates can facilitate intimate coupling to biological tissue surfaces with complex surface texture, such as the brain (**Figure 4**a).

In vivo animal experiments provide evidence for the practical use of this new class of devices. Specifically, sutures that use silk substrates were evaluated in anaesthetized mouse models. After anesthesia delivery, the dorsal side was wiped with alcohol at the incision site with 70% ethanol and the incision was sutured with a customized 16-gauge needle and the smart suture to seal the wound.

Incisions made through the dorsal epidermal layer allowed partial implantation of the Pt temperature sensor strip, as shown in the left frame of Figure 4b. No leakage currents were observed and temperature measurements showed stable values around ~26.5 °C. The right frame of Figure 4b shows an image of sensors after removal of the partially implanted strip from the animal body. The implanted part shows entanglement that results from the high flexibility that follows dissolution of the silk. Some amount of un-implanted silk, however, remains and maintains the original shape of the strip, which facilitates handling. The same experiment is performed with Pt temperature sensors (Figure 4c). The left

Experimental Section

Fabrication of Silicon NM Temperature Sensors: The fabrication began with spin coating a thin polyimide film (PI, ~1.2 µm, Sigma Aldrich, USA) on top of a sacrificial layer of poly(methylmethacrylate) (PMMA, 100 nm, MicroChem, USA) on a handle wafer. Doped single crystalline Si NMs (300 nm) were then transfer printed from a source wafer (n-type SOI wafer, SOITEC, France) to the PI film. The transferred Si NMs were etched to define active regions of pn diodes by using patterns defined by photolithography and reactive ion etching (RIE). Evaporating metal films (Cr/Au, 5 nm/150 nm) followed by photolithography and wet etching formed metal interconnections between the pn diodes and an external DAQ system. A top insulation layer was formed by spin coating of a thin overcoat of epoxy (~1.5 µm). Oxygen reactive ion etching (RIE) defined the overall dimensions of the strip, as shown
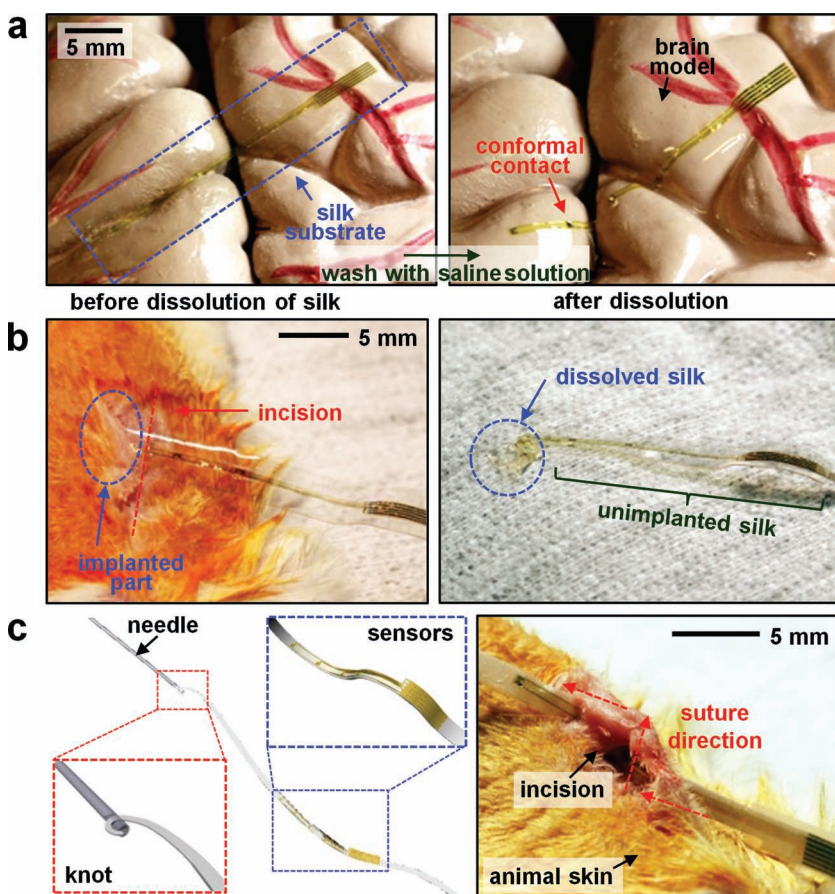
Figure 4. Applications of thin, instrumented suture strips. a) Representative device on a plastic model of the human brain before (left frame) and after (right frame) dissolving a temporary silk substrate. b) Temperature monitoring experiment on an animal model using an instrumented suture strip based on a Pt thermistor on silk substrate. No leakage current is measured before (left frame) and after (center frame) dissolving the silk substrate. c) Temperature monitoring using an instrumented suture strip at the location of an incision on an animal model. Schematic illustration of a suture strip and needle (left frame) and corresponding image after suturing (right frame). Temperature differences inside and outside of the epidermis can be monitored by suturing the incision.

in the top frame of Figure 1b. Transfer printing to a polyester substrate coated with PDMS or a silk substrate, and connecting an ACF cable for external wiring to a DAQ completed the process. For enhanced adhesion, a thin bilayer of Ti/SiO$_2$ (3 nm/30 nm) can be deposited onto the polyester or silk.

Fabrication of Pt Temperature Sensors: The overall shapes and fabrication procedures were similar to those used for the silicon devices. For temperature sensing, however, Pt resistors, instead of Si NM p-n diodes, were located in the island region. Thin layers of Ti/Pt (5 nm/50 nm) deposited with an electron beam (e-beam) evaporator on patterns of photoresist, followed by lift-off formed the Pt resistors. Deposition of Cr/Au (5/150 nm) established interconnection bus lines to each temperature sensor. Surface treatment of the PI with UV/Ozone or deposition of a thin silicon dioxide (SiO$_2$) layer (~50 nm) on top of the PI improved the adhesion of the Pt. Additional encapsulation with thin films of epoxy formed insulation layers to prevent electrical leakage currents. The final device is shown in Figure 1c. The steps for transfer printing and connecting to ACF were the same as those for the silicon NM devices.

Fabrication of Au Heaters: The overall shapes and fabrication procedures were similar to those for the Pt devices. After deposition of Cr/Au (5/150 nm) by electron beam evaporation, wet chemical etching defined patterns of Au for resistive heaters. Final passivation with films of epoxy and etching to define the strip geometries completed the fabrication. The resulting device is shown in the bottom frame of Figure 1b. The steps for transfer printing and connecting to ACF were the same as those for the silicon NM devices.

Silk Preparation: The purification of silk fibroin from Bombyx mori cocoons initially involved removal of sericin, a water-soluble glycoprotein that binds fibroin filaments, by boiling the cocoons in a 0.02 M aqueous solution of sodium carbonate for 30 min. The resulting fibroin bundle was dried and then dissolved in a 9.3 M aqueous solution of lithium bromide at 60 °C for 4 h. The lithium bromide salt was then extracted through a water-based dialysis process over several days. The resulting solution was centrifuged and filtered via syringe based micro-filtration (5 μm pore size, Millipore Inc., Bedford, MA) to remove any remaining particulates. This process enables the production of ~6.5% w/v silk fibroin solution with minimal contaminants and reduced scattering for optical applications. After production of the silk fibroin solution, 10 mL of the solution was cast on 4-inch Si wafers and allowed to crystallize in air (~12 h). The resulting films were then removed from the substrate and were approximately 50 μm thick.

Animal Experiments: All procedures were carried out under approved animal protocols. A female Balb/c mouse was anaesthetized with an intraperitoneal injection of a mix of ketamine–xylazine. The depth of anaesthesia was monitored by palpebral and withdrawal reflexes to confirm that the animal had reached 'stage 3' of anaesthesia. Once the animal was lightly anaesthetized, the dorsal area was shaved and scrubbed with alcohol (70% ethanol) at the incision site, followed with a betadine surgical scrub. To validate the performance of sutures in real conditions, the incision opened during surgery was closed with a customized 16-gauge needle and three passes with the temperature sensing suture were carried out to seal the wound. We then verified the operation of the temperature sensors in the animal. In all instances, the incisions were carried out on the dorsal side of the mouse and the suturing was carried out across the dermal layers above the musculature.

[1] D. L. Steed, *Plast. Reconstr. Surg.* **2006**, *117*, 143S.

[2] S. Rothenburger, D. Spangler, S. Bhende, D. Burkley, *Surgical Infections* **2002**, *3*, s79.

[3] A. Lendlein, R. Langer, *Science* **2002**, *296*, 1673.

[4] T. Sekitani, U. Zschieschang, H. Klauk, T. Someya, *Nat. Mater.* **2010**, *9*, 1015.

[5] M. H. Chiu, W. L. Cheng, G. Muthuraman, C. T. Hsu, H. H. Chung, J. M. Zen, *Biosens. Bioelectron.* **2009**, *24*, 3008.

[6] J. A. Rogers, M. G. Lagally, R. G. Nuzzo, *Nature* **2011**, *477*, 45.

[7] J. Viventi, D. H. Kim, L. Vigeland, E. S. Frechette, J. A. Blanco, Y. S. Kim, A. E. Avrin, V. R. Tiruvadi, S. W. Hwang, A. C. Vanleer, D. F. Wulsin, K. Davis, C. E. Gelber, L. Palmer, J. Van der Spiegel, J. Wu, J. L. Xiao, Y. G. Huang, D. Contreras, J. A. Rogers, B. Litt, *Nat. Neurosci.* **2011**, *14*, 1599.

[8] D. Haemmerich, P. F. Laeseke, *Int. J. Hyperther.* **2005**, *21*, 755.

[9] J. S. Petrofsky, D. Lawson, H. J. Suh, C. Rossi, K. Zapata, E. Broadwell, L. Littleton, *Diabetes. Technol. The.* **2007**, *9*, 535.

[10] C. J. Gannon, P. Cherukuri, B. I. Yakobson, L. Cognet, J. S. Kanzius, C. Kittrell, R. B. Weisman, M. Pasquali, H. K. Schmidt, R. E. Smalley, S. A. Curley, *Cancer* **2007**, *110*, 2654.

[11] S. W. Choi, Y. Zhang, Y. N. Xia, *Angew. Chem., Int. Ed.* **2010**, *49*, 7904.

[12] O. Gonzalez, J. H. Maddocks, *Proc. Natl. Acad. Sci. USA* **1999**, *96*, 4769.

[13] M. J. Kluger, *Proc. Nutr. Soc.* **1989**, *48*, 337.

[14] S. K. Park, Y. H. Kim, J. I. Han, D. G. Moon, W. K. Kim, *Thin Solid Films* **2003**, *429*, 231.

[15] W. Y. Chang, T. H. Fang, S. H. Yeh, Y. C. Lin, *Sensors* **2009**, *9*, 1188.

[16] F. Iacopi, Y. Travaly, M. Van Hove, A. M. Jonas, J. M. Molina-Aldareguia, M. R. Elizalde, I. Ocana, *J. Mater. Res.* **2006**, *21*, 3161.

[17] J. Lee, J. A. Wu, M. X. Shi, J. Yoon, S. I. Park, M. Li, Z. J. Liu, Y. G. Huang, J. A. Rogers, *Adv. Mater.* **2011**, *23*, 986.

[18] S. P. Lacour, S. Wagner, Z. Y. Huang, Z. Suo, *Appl. Phys. Lett.* **2003**, *82*, 2404.

[19] J. Brelle, A. Blatter, R. Ziegenhagen, *Platinum Met. Rev.* **2009**, *53*, 189.

[20] F. H. Gojny, M. H. G. Wichmann, U. Kopke, B. Fiedler, K. Schulte, *Compos. Sci. Technol.* **2004**, *64*, 2363.

[21] E. Tschegg, K. Humer, H. W. Weber, *Cryogenics* **1991**, *31*, 878.

[22] L. U. Devi, S. S. Bhagawan, S. Thomas, *J. Appl. Polym. Sci.* **1997**, *64*, 1739.

[23] L. P. A. Burgess, G. V. Morin, M. Rand, J. Vossoughi, J. O. Hollinger, *Arch. Otolaryngol. Head. Neck. Surg.* **1990**, *116*, 798.